Epidermal cell fusion promotes the transition from an embryonic to a larval transcriptome in *C. elegans*

Owen H. Funk, Daniel L. Levy*, David S. Fay*

Department of Molecular Biology, University of Wyoming, Laramie, WY 82071, USA

*Corresponding authors:

David S. Fay
University of Wyoming
Department of Molecular Biology
1000 E. University Avenue
Laramie, WY 82071
Phone: 307-343-0385 (cell)
Fax: 307-766-5098
E-mail: davidfay@uwyo.edu

Daniel L. Levy
University of Wyoming
Department of Molecular Biology
1000 E. University Avenue
Laramie, WY 82071
Phone: 307-417-0354
Fax: 307-766-5098
E-mail: dlevy1@uwyo.edu

Abstract

Cell fusion is a fundamental process in the development of many multicellular organisms but its precise role in gene regulation and differentiation remains largely unknown. The *Caenorhabditis elegans* epidermis, which is comprised of multiple syncytial cells in the adult, represents a powerful model for studying cell fusion in the context of animal development. The largest of these epidermal syncytia, hyp7, integrates 139 individual nuclei through processive cell fusion mediated by the fusogenic protein EFF-1. To explore the role of cell fusion on developmental progression and associated gene expression changes, we conducted transcriptomic analyses of *eff-1* fusion-defective *C. elegans* mutants. Our RNAseq findings showed widespread transcriptomic changes including the enrichment of epidermal genes and molecular pathways involved in epidermal function during development. Single-molecule fluorescence *in situ* hybridization further validated the observed altered expression of mRNA transcripts. Moreover, bioinformatic analysis suggests that fusion may play a key role in promoting developmental progression within the epidermis. Our results underscore the significance of cell–cell fusion in shaping transcriptional programs during development.

Summary Statement

eff-1 meditated cell fusion drives transcriptomic progression from an embryonic to larval state in the *C. elegans* epidermis, without which developmental progression is delayed.

Key Words

Cell Fusion, EFF-1, *C. elegans* Development, Epidermis, Syncytia, Transcription

Introduction

Multinucleate syncytial cells are evolutionarily conserved and are found throughout the tree of life in physiologically healthy tissues and in disease states such as cancer (1-6). The need for a syncytium varies among organisms and tissues; multiple nuclei may be required to metabolically support larger cells or to facilitate the rapid production of large amounts of mRNA for developmental processes or in response to extracellular cues (7-

11). There are multiple paths by which multinucleate syncytia arise, including cell–cell fusion of multiple mononucleate cells (1, 12-15). Cellular fusion necessarily merges the cytoplasm of two distinct cells, but how mixing of cytoplasmic factors changes the regulatory environment of individual nuclei and thus affects the transcriptome within a newly formed syncytium is poorly understood (16-19).

The *C. elegans* epidermis (also termed hypodermis) is an excellent model to address questions related to the function of syncytial nuclei. *C. elegans* has a well-characterized and largely invariant cell lineage in which over a third of somatic nuclei ultimately reside within syncytial cells (14, 20). The adult worm epidermis is composed of multiple syncytial cells, the largest of which is hyp7, which surrounds most of the adult body (14). hyp7 forms through progressive rounds of cell fusion, beginning with 23 embryonic fusion events that create the initial larval hyp7 prior to hatching. This process is completely dependent on cell–cell fusion mediated by the fusogen EFF-1 and is followed by the addition of 116 additional nuclei through EFF-1–mediated fusion events during larval development (21-23).

eff-1 was initially discovered through genetic screens as the lone factor that is both necessary and sufficient to induce cell fusion in the *C. elegans* epidermis (22, 23). Mutations in *eff-1* lead to the disruption of embryonic fusion events in the developing hypodermal syncytium, leaving the hypodermal progenitors unfused and embryonic cell boundaries intact. *eff-1* mutant worms exhibit variable morphological and developmental defects, highlighting the importance of cell fusion for proper body morphogenesis (21, 23-25).

Here we explore the role of embryonic cell fusion in gene expression and differentiation in the developing epidermal syncytium through RNAseq of worms containing reduction-of-function mutations in EFF-1, which block most epidermal fusion events in the embryo. Reduced fusion led to an increase in embryo-associated gene transcripts concurrent with a decreased expression of larval-associated transcripts in genes expressed specifically in the epidermis. These findings suggest a developmental delay

in the acquisition of epidermal cell fates and a possible role for cell fusion in activating gene regulatory programs associated with epidermal differentiation, adding to the growing list of functions for cell fusion and syncytialization.

Results and Discussion

eff-1–mediated cell fusion is essential for normal developmental progression and morphology in *C. elegans*

The discovery of EFF-1 as the primary fusogen governing most epidermal cell fusions in *C. elegans* originated from classical mutagenesis screens (21-23). This included two mutations—P183L (*hy21*) and S441L (*oj55*)—that exhibit variable penetrance fusion defects and temperature sensitivity. Based on available data, both mutations appear to be partial reduction-of-function mutations rather than complete knockouts and would be expected to contain background mutations as a result of the mutagenesis, as well as additional differences in strain backgrounds (23). We therefore generated strains containing an *eff-1* putative null mutation using CRISPR (P37Stop), which places two stop codons in exon 1 that is present in all *eff-1* isoforms (**Fig. 1A**). As discussed below, this precise modification may lead to a stronger reduction of function of *eff-1* as compared with the historical alleles and allows for a cleaner comparison to our wild type (WT; N2) fusion-competent control.

Consistent with previous reports, *eff-1*(P37Stop) mutants displayed characteristic morphological defects, including a bulging anterior region, tail spike abnormalities, and a dumpy (Dpy) phenotype that persisted into adulthood (**Fig. 1B**) (23). To visualize fusion defects in *eff-1* mutants we imaged apical junctions using AJM-1::GFP and confirmed that *eff-1(*P37Stop) mutants have an unfused epidermis that persists into adulthood (**Fig. 1C,D**). We note that the original characterization of the *eff-1* mutants reported a complete lack of fusion during late embryonic stages but with partial fusion occurring during larval development at temperatures below 25°C (23).

We next characterized the developmental timing of *eff-1*(P37Stop) and the historical mutants from hatching to first molt and to reproductive adulthood. Like *eff-1*(P183L) and

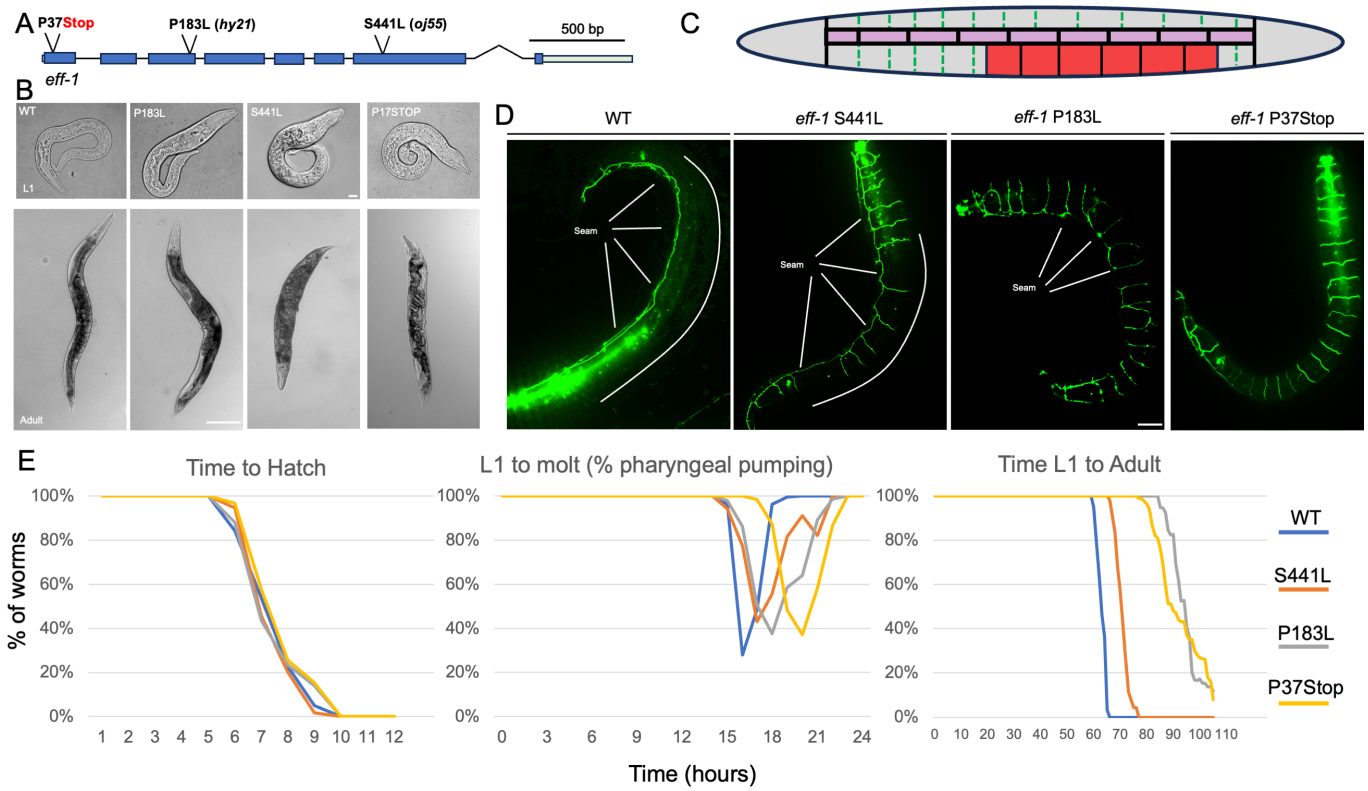

Figure 1. *eff-1* mutant worms display morphological defects and developmental delay. A) *eff-1* gene locus with CRISPR edit P37Stop and mutant alleles P183L (*hy21*) and S441L (*oj55*) indicated. B) Brightfield imaging of L1 and adult N2 and *eff-1* mutants as indicated. Scale bars: L1, 10µm; adult, 100µm. C) Schematic of L1 hypodermis with *eff-1*–mediated fusion events marked with dashed green lines, seam-cells in pink and P cells in red. D) Representative images of AJM-1::GFP fluorescence, a marker of apical cell–cell junctions in the epidermis, in N2 (WT) and *eff-1* mutant L1 larvae; lateral seam cells are labeled. E) Quantification of developmental timepoints in N2 and *eff-1* mutants. Time to first molt was measured via the cessation of pharyngeal pumping. Time to hatch and adulthood was measured by locomotion and sexual maturity, respectively. n of > 40 per condition and timepoint.

eff-1(S441L), *eff-1*(P37Stop) exhibited developmental delays in the time to first molt and the time to reach adulthood, although the delays in *eff-1*(P183L) and *eff-1*(P37Stop) appeared more pronounced than *eff-1*(S441L) (**Fig. 1E**). Additionally, all three *eff-1* mutants were less synchronous than WT and we observed a low frequency of larval arrest in the *eff-1*(P183L) and *eff-1*(P37Stop) mutants.

Disruption of cell fusion in embryonic development leads to consistent, widespread transcriptomic changes in *eff-1* mutants

129 The transition from embryo to larva is accompanied by widespread transcriptional
130 rewiring as the newly hatched L1s begin locomotion and feeding and as many tissues
131 and cell types acquire their terminal post-mitotic fate (26-29). To examine the role of cell
132 fusion in the embryonic-to-larval transition, we conducted RNAseq on synchronized
133 early L1-stage WT, *eff-1*(P37Stop), *eff-1*(S441L), and *eff-1*(P183L) L1 animals. For *eff-*
134 *1*(P37Stop), differential expression analysis revealed 2046 upregulated and 912
135 downregulated differentially expressed genes (DEGs) relative to WT with a false-
136 discovery rate (FDR) cutoff of <0.05 and $\log_2$(fold change) cutoff of >0.5 or <-0.5 (**Fig.**
137 **2A, File S1**). Additionally, we found 3534 upregulated and 2558 downregulated DEGs in
138 *eff-1*(S441L) mutants, and 6499 up and 6829 down DEGs in *eff-1*(P183L) mutants (**Fig.**
139 **S1A, File S1**). The larger number of DEGs observed in the previously isolated mutant
140 strains is not entirely unexpected given that these strains were generated by random
141 mutagenesis and that the parental strains used to generate these alleles may differ
142 somewhat from our N2 reference strain. As such, some of the transcriptomic changes in
143 these strains are likely attributable to background variations.
144
145 Despite potential background differences, we observed a strong overlap between *eff-*
146 *1*(P37Stop), *eff-1*(S441L), and *eff-1*(P183L), with 958 shared DEGs that were
147 differentially regulated in the same direction (293 downregulated and 665 upregulated)
148 (**Fig. 2B,C**). Furthermore, $\log_2$-transformed fold-change data for the top DEGs from all
149 three mutant strains also showed high concordance, with top genes shifting in the same
150 direction regardless of the *eff-1* mutation (**Fig. 2D**). Euclidian distances between
151 samples also confirmed transcriptome-wide similarities between *eff-1* point mutations
152 and P37Stop as compared with WT (**Fig. S1B**). Notably, the P183L transcriptome
153 appears highly divergent, even more so than the P37Stop despite being only a point
154 mutation. We suspect this is due to additional background mutations introduced in the
155 original derivation of this strain, further highlighting the utility of a clean, engineered
156 knockout.
157
158 Taken together, these data indicate a shared core transcriptomic response to the
159 absence of epidermal cell fusion in L1 larvae, regardless of the specific *eff-1* allele or

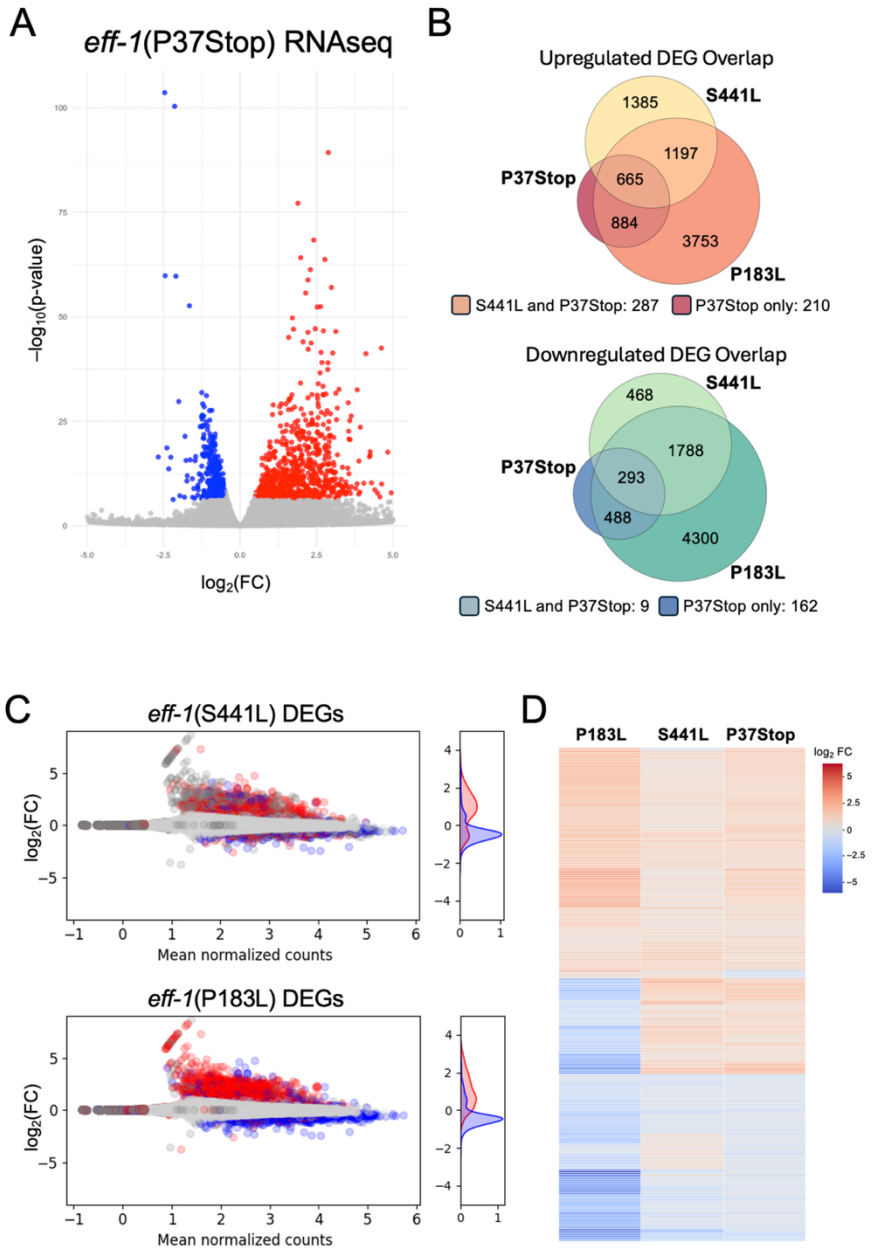

Figure 2. RNAseq of multiple *eff-1* mutants indicates a common transcriptome response to fusion disruption.

A) Volcano plot of top DEGs (downregulated in blue, upregulated in red) for *eff-1*(P37Stop). B) Overlap of significant (adjusted p-value < .05, $\log_2$FC < -0.5 or > 0.5) DEGs from P37Stop, S441L, and P183L. C) MA (minus average; Bland-Altman) plot of *eff-1*(P37Stop) mutants with upregulated (red) and downregulated (blue) DEGs from S441L and P183L relative to WT. DEGs up- and downregulated in one mutant are more often found differentially expressed in the same direction in the other mutant. Right-side inset shows density of colored (shared DEGs) points D) Heatmap of $\log_2$-transformed fold changes (FCs) of top 200 DEGs shared between the *eff-1* mutants.

genetic background. The substantial overlap in both the identity of DEGs and the directionality of their fold changes across all *eff-1* mutant conditions suggests a conserved transcriptional signature linked directly to the disruption of epidermal syncytialization. This highlights a fundamental set of gene expression changes that is consistently triggered by the failure of cells to fuse in the developing epidermis.

Disruption of *eff-1*–mediated fusion alters epidermal cell expression

The hyp7 syncytium has many functions including the production of a new cuticle at each molting cycle, which occurs via the synthesis and secretion of apical extracellular matrix (aECM) proteins that include many collagens (30-34). Consistent with a disruption of these functions, Gene Ontology (GO) enrichment analysis showed a substantial number of terms associated with epidermal-specific processes, specifically extracellular proteins involved in molting and cuticle production (e.g., structural constituent of cuticle, collagen-containing ECM, etc.) (**Fig. 3A**). These findings support the notion that normal hypodermal differentiation and function are disrupted or significantly delayed in *eff-1* mutants. Combined with the tissue enrichment analysis (**Fig. 3C**), these data suggest that the changes in gene expression observed in fusion-defective worms occur primarily among genes and pathways associated with the epidermis and epidermal functions relative to other cell and tissue types. To this point, intersecting all shared DEGs with genes with detectable expression in the L1 epidermis found 89.6% of DEGs were present, strengthening the claim that most of genes found to change their expression are present in the larval epidermis.

In addition to the curated set of GO terms on Wormbase, we noted an enrichment in embryonic precuticle- or “sheath”-associated genes that accompanied the decrease in L1-specific genes (**Fig. 3B**). The sheath is the first precuticle formed during embryonic development prior to secretion of the first cuticle (35-38)**.** The presence of precuticle gene expression at the L1 stage in *eff-1* mutants suggests a delay in the transition from precuticle to cuticle gene expression programs. This finding, coupled with the observed downregulation of L1-specific collagen genes, points toward an overall impairment or

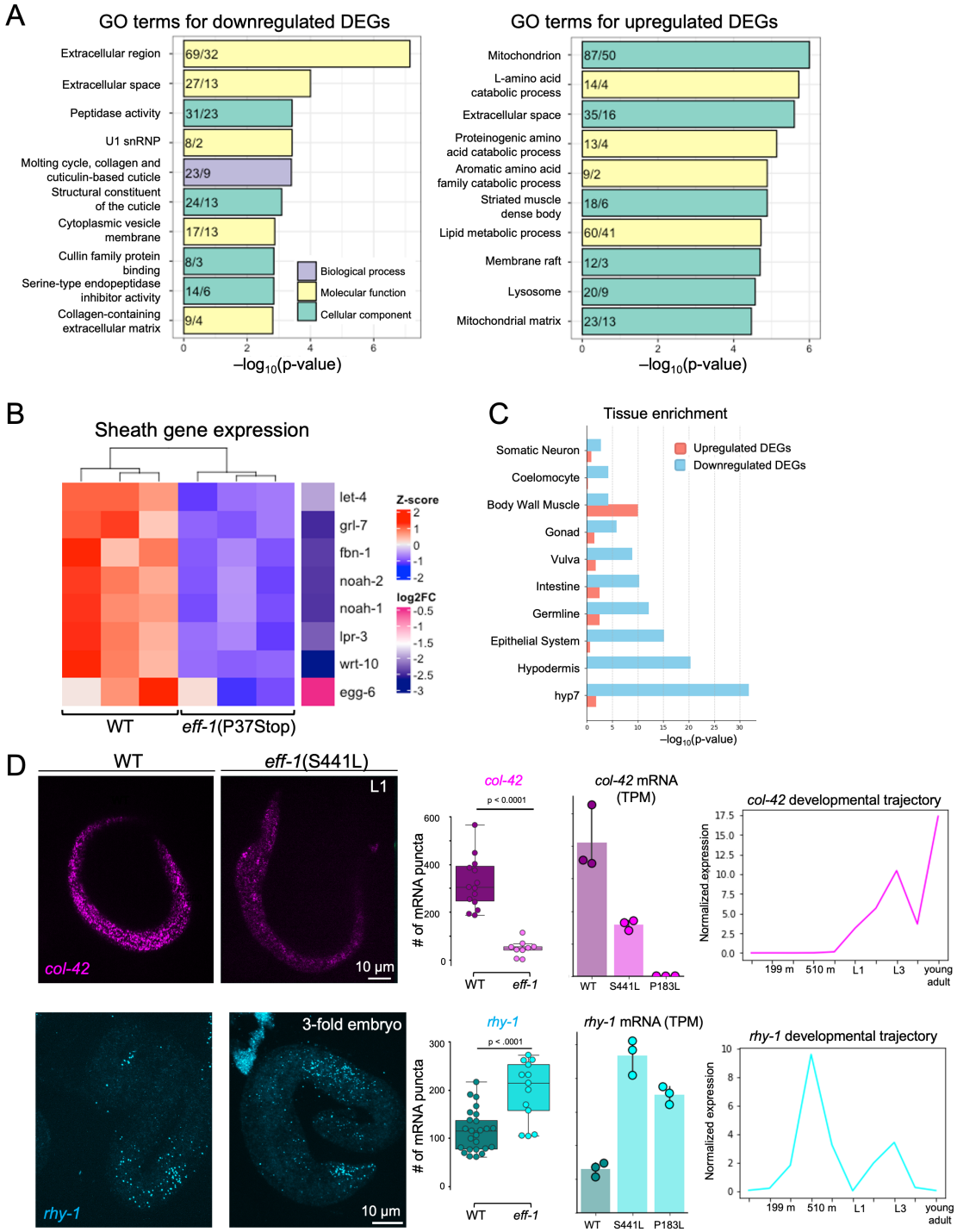

Figure 3. The null *eff-1* mutation affects diverse functions.

A) GO term enrichment using topGO with DEGs from *eff-1*(P37Stop) RNAseq. Colors indicate GO term category as shown in the key. Numbers associated with each bar indicate the observed/expected genes for each GO term displayed. B) Heatmap of z-score–transformed mean expression and $\log_2$(FC) values for selected sheath genes in WT and *eff*-1(P37Stop) L1s. C) Tissue enrichment analysis of DEGs based on gold-standard small-scale enrichment

experiments (37). DEGs were intersected with lists of tissue-specific genes, and p-values were calculated based on hypergeometric significance. D) Representative images of *col-42* and *rhy-1* smiFISH hybridization in WT and e*ff-1*(S441L) L1s and 3-fold-stage embryos, respectively. mRNAs were quantified based on the number of fluorescent puncta. RNAseq counts (transcripts per million; TPM) for WT and *eff-1* mutants for *col-42* mRNA at L1 larvae and rhy-1 mRNA in embryos. Developmental trajectory of *col-42* and *rhy-1* expression in WT animals taken from modENCODE expression data (39). Error bars represent standard error; minimum of nine animals per condition.

delay in the transcriptional wiring necessary for proper L1 epidermal maturation and function.

To independently validate and visualize changes in the expression of specific DEGs, we used single-molecule inexpensive fluorescence *in situ* hybridization (smiFISH) of two DEGs identified in our RNAseq data, *col-42* and *rhy-1*. *col-42* encodes a structural collagen largely restricted to larvae and adults and was significantly downregulated in both *eff-1*(S441L) and *eff-1*(P183L) mutants (**Fig. 3D**). *col-42* is expressed during early larval development, and smiFISH imaging showed almost no detectable signal in *eff-1* mutants at L1 (**Fig. 3D**). Conversely, *rhy-1* is a transmembrane acyltransferase that is expressed in the embryonic epidermis (40, 41). Consistent with the transcriptomic data, the number of *rhy-1* mRNA fluorescent puncta was also elevated in *eff-1* mutants (**Fig. 3D**).

Although large changes in the transcriptomes of *eff-1* mutants were evident, such changes may be due to direct or indirect effects caused by the disruption of epidermal cell functions. To distinguish between these possibilities, we looked for overlap between gold-standard lists of tissue-specific genes from small-scale single-tissue experiments and the *eff-1* DEGs (42). This analysis showed a significant enrichment among downregulated DEGs for transcripts associated with the hyp7 syncytium, hypodermis, and epithelial system, over other non-syncytial tissues (**Fig. 3C**), consistent with a model in which unfused hyp7 progenitors fail to upregulate genes found in the L1 syncytial hypodermis. This suggests that the observed transcriptomic changes are, in large part, the direct consequence of an unfused epidermis rather than of a systemic developmental delay. Collectively, our data support the central finding that fusion plays a

261 critical role in promoting the timely differentiation and function of the epidermis based on
262 hallmark changes in gene expression.
263
264 ***eff-1* mutant transcriptional changes are consistent with a developmental delay**
265 In addition to shared pathways and functions associated with the DEGs isolated across
266 *eff-1* mutations, we found a striking enrichment in the DEGs associated with the
267 transition from embryonic to larval development. By examining the developmental
268 trajectory of DEGs at timepoints throughout the WT worm lifecycle from modENCODE
269 (39, 43), we found an enrichment in L1-associated genes in the downregulated DEG
270 set, along with upregulated DEGs showing substantial enrichment for genes normally
271 expressed in the late embryo (**Fig. 4A, D**). Furthermore, genes that were not
272 differentially expressed (FDR > 0.05) in the *eff-1* mutants were predominantly those for
273 which expression levels remain relatively stable across normal development.
274 Collectively, these observations strongly suggest that the normal transcriptional shift
275 from late-embryonic to L1 larval gene expression programs is substantially delayed in
276 worms deficient for EFF-1–mediated fusion.
277
278 To further investigate the hypothesis that *eff-1* mutant L1s inappropriately maintain high
279 expression of embryonic genes while failing to upregulate larval-specific genes, we
280 performed a linear regression analysis. This analysis used WT expression data across
281 multiple embryonic and larval timepoints to define gene sets that are developmentally
282 upregulated or downregulated during the transition from late-embryonic to larval stages.
283 We then compared the average fold changes of these developmentally dynamic gene
284 sets to *eff-1*(P37Stop) mutants. This comparison revealed a net increase in the
285 expression of developmentally downregulated (i.e., typically embryonically enriched)
286 genes and a corresponding decrease in the expression of developmentally upregulated
287 (i.e., typically larvally enriched) genes, irrespective of whether individual genes met the
288 strict criteria for differential expression (**Fig. 4B**). This broader analysis reinforces the
289 conclusion that the absence of cell fusion leads to a significant delay in the acquisition
290 of the appropriate L1 transcriptome.
291

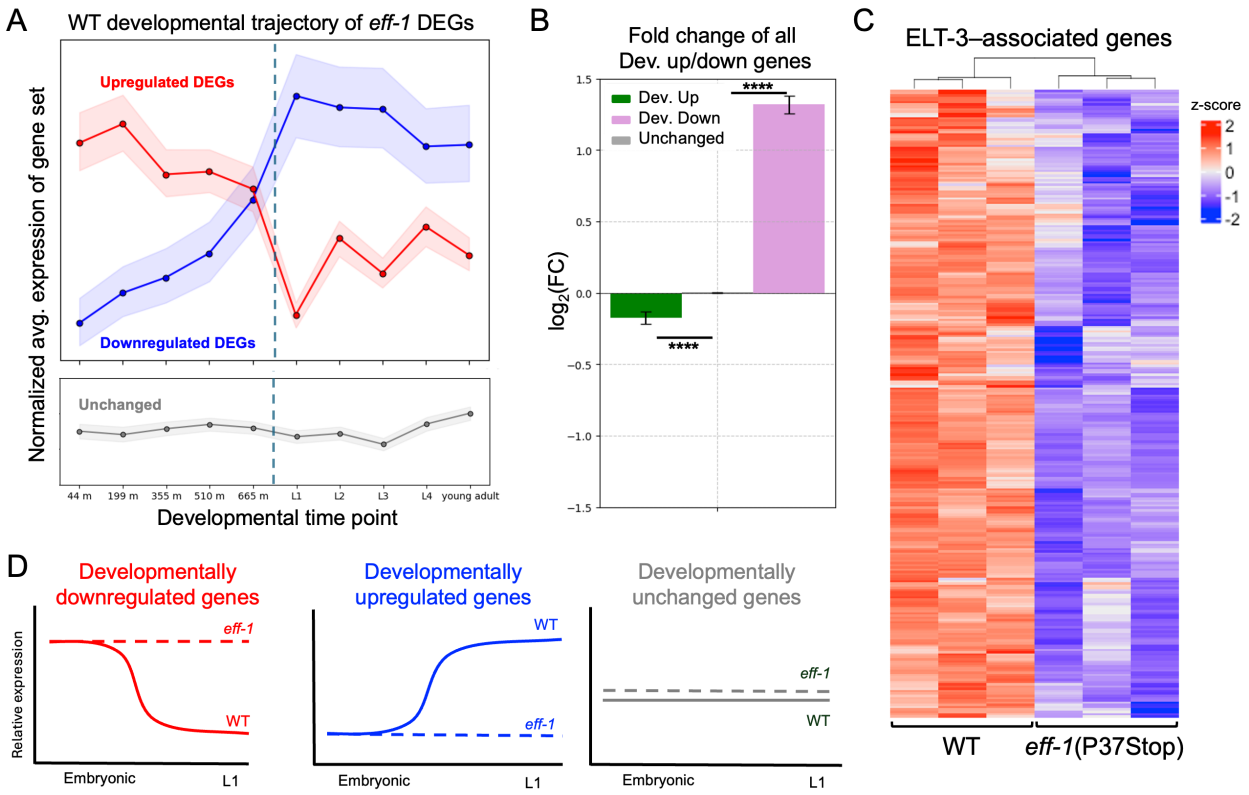

Figure 4. Fusion mutants fail to acquire the L1 epidermal transcriptome. Normal (WT) developmental trajectories of genes that were upregulated (red) or downregulated (blue) in *eff-1* mutants. Shaded region denotes 95% confidence interval. Fusion-defective transcriptomes show a marked increase in embryonic transcripts with a concurrent downshift in larval-associated transcripts. Dashed line indicates an approximate hatching time of 800 min. B) Genes were binned using a linear regression of modENCODE data to determine transcripts that went up (green), down (purple) or stayed consistent (gray) across normal WT development. Average $\log_2$–transformed fold change data of *eff-1*(P37Stop) RNAseq data for each category of genes are shown. Error bars represent standard error, and p-values calculated using Mann-Whitney U test, ****P < .00001. C) Heatmap of z-score normalized DEG expression for genes identified as ELT-3 regulated from the TF2DNA dataset (49). D) Schematic of WT and *eff-1* mutant gene expression profiles across development, showing a lack of transition from the embryonic to larval transcriptome in fusion defective *eff-1* mutants.

The transition from an embryonic to larval transcriptome is facilitated by many transcription factors, including ELT-3, an embryonically enriched GATA transcription factor with roles in the transcriptional activation of epidermis-specific genes and developmental pathways (44-46). Previously, an *elt-3* reporter construct was found to be expressed in only a subset of hypodermal precursor cells, and thus it has been used as a reporter for fusion, or lack thereof, in *eff-1* mutant worms (47). Intriguingly, we found a

312 large swath of ELT-3 regulated genes identified through the TF2DNA database as
313 significantly downregulated in *eff-1* mutant worms (**Fig. 4C**). Examination of the ELT-3
314 chromatin immunoprecipitation sequencing (ChIPseq) signal across all up, down, and
315 unchanged genes also showed an enrichment of downregulated genes (**Fig. S2**). The
316 observed downregulation of ELT-3 target genes in *eff-1* mutants provides a potential
317 mechanistic link between the failure of cell fusion and the observed developmental
318 delay. Namely, cell fusion may be necessary for the appropriate stage-specific activity of
319 key developmental regulators such as ELT-3, which may be expressed in only a subset
320 of cells contributing to epidermal syncytia.

321

322 Taken together, our work underscores the critical role of EFF-1–mediated cell fusion in
323 the developmental progression of *C. elegans* and highlights its importance for the timely
324 activation of the L1 larval transcriptome. Our findings suggest that the process of fusion
325 itself may be a key mechanistic trigger promoting the shift from the embryonic to the L1
326 transcriptional landscape in fusion-driven syncytia such as hyp7. Although these results
327 highlight the importance of syncytial formation for the proper expression of
328 developmental genes, precisely how fusion orchestrates transcriptional maturation
329 remains an open question. Future investigations will be needed to unravel the molecular
330 mechanisms involved and to identify specific factors that may drive the identity and
331 transcriptional programs of developing syncytial nuclei.

332

333 **Materials and Methods**

334 **Strains used and maintenance**

335 *C. elegans* strains were maintained according to standard protocols and were
336 propagated at 22°C. The two *eff-1* mutant strains used here were WH171 (*eff-1*(*oj55*);
337 jcIs1 *[ajm-1::GFP + unc-29(+) + rol-6(su1006)]*) and BP76 (*eff-1*(*hy21*); jcIs1 *[ajm-*
338 *1::GFP + unc-29(+) + rol-6(su1006)]*). MH1384 (*[kuIs46 (ajm-1::GFP; unc-119(+))]*) was
339 used to compare WT AJM-1::GFP expression to that in e*ff-1* mutants. The P37Stop
340 strain as generated using CRISPR via the method described in Ghanta et. al 2021 (48).
341 Briefly, RNPs loaded with gRNA (GGTGTCTTGGAACAGTGTGG) were injected along

342 with repair template designed to add two stop codons along with an SpeI recognition
343 site into the gonads of animals expressing *kuIs46*[AJM-1::gfp] and *bqSi640*[*dpy-*
344 *7p*::FRT::mCherry::*his-58*::FRT::GFP::*his-58*].

345 **Developmental timing analysis**

346 Time to hatch was determined by plating young adult worms, allowing them to lay eggs
347 for 2 hours, and then removing the adults and measuring the percentage of unhatched
348 eggs that remained over time. Time to molt was determined by plating synchronized L1
349 larvae and watching for cessation of pharyngeal pumping to mark the beginning of the
350 L1–L2 molt. Time to adulthood was measured by plating synchronized L1 larvae and
351 noting the presence of embryos in the gonads. All experiments were carried out at 22°C.
352

353 **Microscopy**

354 Confocal images for **Fig. 1** were taken using CellSens on an Olympus Spin-SR,
355 Spinning Disc, Super Resolution System using an inverted Olympus IX83 microscope
356 and Yokogawa W1 spinning disc. smiFISH images were taken of worms fixed in
357 methanol/acetone as described (49). Larvae for **Fig. 1** images were prepared in 10 mM
358 levamisole on 3% agarose pads.
359

360 **RNA isolation and RNAseq**

361 L1s were synchronized by bleaching gravid adults and allowing embryos to arrest in M9
362 buffer. L1s were spun down and lysed for RNA collection via the Direct-zol kit from
363 Zymo. RNA quality was confirmed using an Agilent TapeStation with minimum RINs
364 (RNA Integrity Number) of 8.0. mRNA libraries were constructed using TruSeq Library
365 Prep Kits from Illumina and were sequenced on an Illumina Nextseq P3 flow cell.
366

367 **Transcriptomic analysis**

368 Paired-end reads were processed as follows. Low-quality reads were filtered using
369 fastp, and their quality was assessed using fastQC (0.12.1). Reads were aligned using
370 STAR and pseudoaligned using Salmon to the *ce11* reference genome, duplicates were
371 removed using picard, and counts were collected using htseq (50-52). Differential
372 expression was determined using DESeq2 (v. 1.42.1), with counts filtered for >1 TPM

373 across all samples . DEGs were defined as genes with a Benjamini-Hochberg adjusted
374 $p < 0.05$ and $\log_2$(fold change) > 0.5 or < –0.5 **, (**processed files in **File S1)**. Heatmaps
375 were generated using the seaborn clustermap() function using Euclidian distance to
376 obtain hierarchal linkages and z-score normalization by rows. Intersectional analysis
377 was done by collecting modENCODE developmental expression data, processed in
378 Hutter and Soh 2016 (39, 43). Upregulated, downregulated, and unchanged
379 classifications were determined by performing a linear regression for expression data
380 across developmental time points and collecting genes with a derived slope of >1
381 (developmentally upregulated) or <–1 (developmentally downregulated). Genes with a
382 derived slope from 1 to –1 were categorized as unchanged. Raw and processed data
383 files can be found through GEO accession: (GSE301850).
384
385 **GO term analysis**
386 GO term enrichment was carried out using topGO (v. 2.54.0) on ontologies from
387 WormBase using the "weight01" algorithm, and significance was assessed with a
388 Fisher's statistic. Genes found to be differentially expressed (FDR < 0.05) in both S441L
389 and P183L were used as the test set, and the background gene set was specified as
390 genes with a base mean TPM of >1 in all three transcriptomes.
391
392 **Tissue enrichment**
393 Gold-standard tissue-specific gene sets were obtained from https://worm.princeton.edu/
394 (42) and compared to DEGs from the *eff-1* mutant RNAseq data. Fischer's exact test
395 was used to calculate enrichment significance.
396
397 **smiFISH**
398 smiFISH was carried out as described (49). Probe sets were designed against *col-42*
399 and *rhy-1* using Oligostan with FLAP-X extensions (53). The FLAP-X secondary probes
400 were labeled with Quasar 670 from Biosearch Technologies. Quantification was done in
401 FIJI by manually drawing designated regions of interest around embryos and L1s of
402 appropriate age and sufficient fixation, thresholding across experimental replicates, and
403 using the "analyze particles" option.

404

405 **ELT-3 ChIPseq analysis**

406 ELT-3–associated genes were obtained from the TF2DNA dataset (54) and compared to
407 our experimentally derived DEGs. L1 ELT-3 ChIPseq data from modENCODE was
408 downloaded as read-depth–normalized bigwig files. Heatmaps were generated
409 with *deeptools* (v 3.5.6) (55). Up- and downregulated gene sets were designated from
410 the *eff-1* P37Stop dataset with the same criteria (adjusted p-value < .05, log2 fold
411 change > 0.5 or < -0.5. Unchanged genes were taken as a random subset of 5000
412 genes with adjusted p-value > .2.

413

414 **Acknowledgements**

415 This work was supported by the National Institutes of Health grants GM136236 and
416 GM125091 (to D.S.F.), GM134885 (to D.L.L.). This project was also supported by an
417 Institutional Development Award (IDeA) from the National Institute of General Medical
418 Sciences of the National Institutes of Health under P20GM103432. We thank Amy Fluet
419 for editing this manuscript, the Nishimura lab for guidance and implementation of
420 smiFISH, the Sundaram and Murray labs for insightful conversation and feedback on
421 the results.

422

423 **Author contributions**

424 Conceptualization, OHF, DLL, DSF; Investigation, OHF; Writing – Original Draft, OHF;
425 Writing – Review & Editing, OHF, DLL, DSF; Funding Acquisition, DLL, DSF;
426 Supervision, DLL, DSF.

427

428

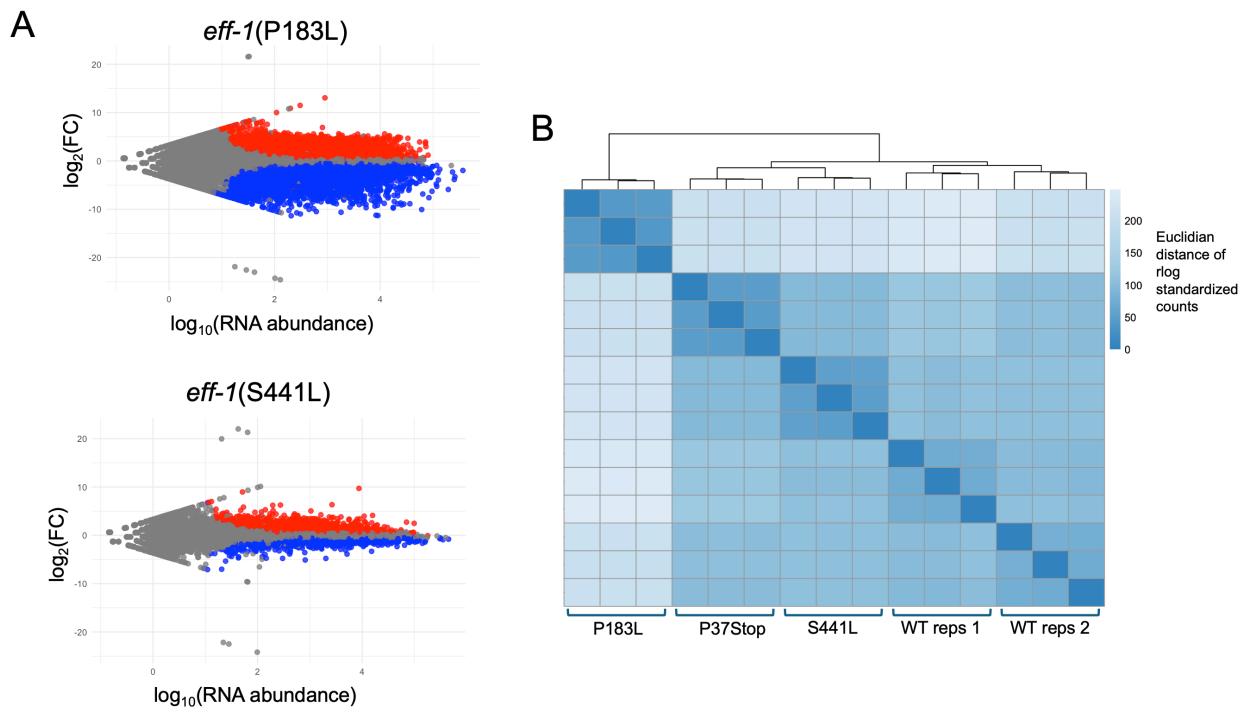

429 **Figure S1. RNAseq of *eff-1* mutants shows substantial overlap in gene expression**
430 **changes.**
431 A) MA plots of *eff-1*(P183L) and *eff-1*(S441L) with DEGs (adjusted $p < 0.05$) in red for
432 upregulated and blue for downregulated. B) Euclidian distance matrix of regularized log
433 transformed RNAseq counts of *eff-1* mutants and WT controls from multiple sequencing runs.
434

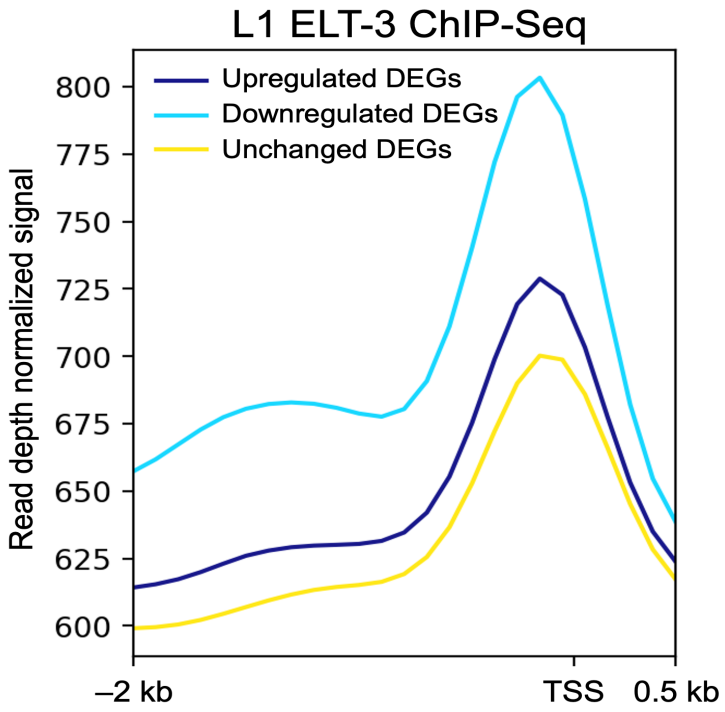

Figure S2. ELT-3 ChIPseq signal across *eff-1* differentially expressed genes.
L1 ELT-3 ChIPseq profile across DEGs from *eff-1*(P37Stop). ELT-3 ChIPseq signal was derived from modENCODE data and plotted for a region spanning 2 kb upstream and 500 bp downstream from the transcription start site (TSS) of upregulated, downregulated, and unchanged genes.

References

1. B. M. Ogle, M. Cascalho, J. L. Platt, Biological implications of cell fusion. *Nat Rev Mol Cell Biol* **6**, 567-575 (2005).
2. S. J. Calvert *et al.*, Studies of the dynamics of nuclear clustering in human syncytiotrophoblast. *Reproduction* **151**, 657-671 (2016).
3. P. J. Brooks, M. Glogauer, C. A. McCulloch, An Overview of the Derivation and Function of Multinucleated Giant Cells and Their Role in Pathologic Processes. *Am J Pathol* **189**, 1145-1158 (2019).
4. L. I. Larsson, B. Bjerregaard, J. F. Talts, Cell fusions in mammals. *Histochem Cell Biol* **129**, 551-561 (2008).
5. S. M. Abmayr, G. K. Pavlath, Myoblast fusion: lessons from flies and mice. *Development* **139**, 641-656 (2012).
6. M. Roper, C. Ellison, J. W. Taylor, N. L. Glass, Nuclear and genome dynamics in multinucleate ascomycete fungi. *Curr Biol* **21**, R786-793 (2011).
7. J. J. Dowling, C. C. Weihl, M. J. Spencer, Molecular and cellular basis of genetically inherited skeletal muscle disorders. *Nat Rev Mol Cell Biol* **22**, 713-732 (2021).
8. M. Cardamone, B. T. Darras, M. M. Ryan, Inherited myopathies and muscular dystrophies. *Semin Neurol* **28**, 250-259 (2008).
9. Y. Iosilevskii, B. Podbilewicz, Programmed cell fusion in development and homeostasis. *Curr Top Dev Biol* **144**, 215-244 (2021).
10. T. L. Orr-Weaver, When bigger is better: the role of polyploidy in organogenesis. *Trends Genet* **31**, 307-315 (2015).
11. O. Deshpande, J. de-Carvalho, D. V. Vieira, I. A. Telley, Astral microtubule cross-linking safeguards uniform nuclear distribution in the Drosophila syncytium. *J Cell Biol* **221** (2022).
12. S. Demin, M. Berdieva, A. Goodkov, Cell-cell fusions and cell-in-cell phenomena in healthy cells and cancer: Lessons from protists and invertebrates. *Semin Cancer Biol* **81**, 96-105 (2022).
13. E. H. Chen, E. Grote, W. Mohler, A. Vignery, Cell-cell fusion. *FEBS Lett* **581**, 2181-2193 (2007).
14. S. Alper, B. Podbilewicz, Cell fusion in Caenorhabditis elegans. *Methods Mol Biol* **475**, 53-74 (2008).
15. P. S. Aguilar *et al.*, Genetic basis of cell-cell fusion mechanisms. *Trends Genet* **29**, 427-437 (2013).
16. M. Kim *et al.*, Single-nucleus transcriptomics reveals functional compartmentalization in syncytial skeletal muscle cells. *Nat Commun* **11**, 6375 (2020).
17. M. J. Petrany *et al.*, Single-nucleus RNA-seq identifies transcriptional heterogeneity in multinucleated skeletal myofibers. *Nat Commun* **11**, 6374 (2020).
18. K. Williams, K. Yokomori, A. Mortazavi, Heterogeneous Skeletal Muscle Cell and Nucleus Populations Identified by Single-Cell and Single-Nucleus Resolution Transcriptome Assays. *Front Genet* **13**, 835099 (2022).

493 19. X. Liu *et al.*, Analysis of cell fate from single-cell gene expression profiles in C.
494 elegans. *Cell* **139**, 623-633 (2009).
495 20. B. Podbilewicz, J. G. White, Cell fusions in the developing epithelial of C. elegans.
496 *Dev Biol* **161**, 408-424 (1994).
497 21. B. Podbilewicz *et al.*, The C. elegans developmental fusogen EFF-1 mediates
498 homotypic fusion in heterologous cells and in vivo. *Dev Cell* **11**, 471-481 (2006).
499 22. G. Shemer *et al.*, EFF-1 is sufficient to initiate and execute tissue-specific cell fusion
500 in C. elegans. *Curr Biol* **14**, 1587-1591 (2004).
501 23. W. A. Mohler *et al.*, The type I membrane protein EFF-1 is essential for
502 developmental cell fusion. *Dev Cell* **2**, 355-362 (2002).
503 24. S. L. Koneru *et al.*, A role for the fusogen eff-1 in epidermal stem cell number
504 robustness in Caenorhabditis elegans. *Sci Rep* **11**, 9787 (2021).
505 25. C. Brabin, P. J. Appleford, A. Woollard, The Caenorhabditis elegans GATA factor ELT-1
506 works through the cell proliferation regulator BRO-1 and the Fusogen EFF-1 to
507 maintain the seam stem-like fate. *PLoS Genet* **7**, e1002200 (2011).
508 26. J. I. Murray *et al.*, Automated analysis of embryonic gene expression with cellular
509 resolution in C. elegans. *Nat Methods* **5**, 703-709 (2008).
510 27. M. E. Boeck *et al.*, The time-resolved transcriptome of C. elegans. *Genome Res* **26**,
511 1441-1450 (2016).
512 28. J. Cao *et al.*, Comprehensive single-cell transcriptional profiling of a multicellular
513 organism. *Science* **357**, 661-667 (2017).
514 29. J. S. Packer *et al.*, A lineage-resolved molecular atlas of. *Science* **365** (2019).
515 30. G. J. Hendriks, D. Gaidatzis, F. Aeschimann, H. Großhans, Extensive oscillatory gene
516 expression during C. elegans larval development. *Mol Cell* **53**, 380-392 (2014).
517 31. M. W. Meeuse *et al.*, Developmental function and state transitions of a gene
518 expression oscillator in Caenorhabditis elegans. *Mol Syst Biol* **16**, e9498 (2020).
519 32. A. D. Chisholm, T. I. Hsiao, The Caenorhabditis elegans epidermis as a model skin. I:
520 development, patterning, and growth. *Wiley Interdiscip Rev Dev Biol* **1**, 861-878
521 (2012).
522 33. I. L. Johnstone, Cuticle collagen genes. Expression in Caenorhabditis elegans.
523 *Trends Genet* **16**, 21-27 (2000).
524 34. A. P. Page, I. L. Johnstone, The cuticle. *WormBook* 10.1895/wormbook.1.138.1, 1-15
525 (2007).
526 35. M. Costa, B. W. Draper, J. R. Priess, The role of actin filaments in patterning the
527 Caenorhabditis elegans cuticle. *Dev Biol* **184**, 373-384 (1997).
528 36. J. R. Priess, D. I. Hirsh, Caenorhabditis elegans morphogenesis: the role of the
529 cytoskeleton in elongation of the embryo. *Dev Biol* **117**, 156-173 (1986).
530 37. V. P. Mancuso *et al.*, Extracellular leucine-rich repeat proteins are required to
531 organize the apical extracellular matrix and maintain epithelial junction integrity in
532 C. elegans. *Development* **139**, 979-990 (2012).
533 38. M. V. Sundaram, N. Pujol, The Caenorhabditis elegans cuticle and precuticle: a
534 model for studying dynamic apical extracellular matrices in vivo. *Genetics* **227**
535 (2024).

536 39. M. B. Gerstein *et al.*, Integrative analysis of the Caenorhabditis elegans genome by
537 the modENCODE project. *Science* **330**, 1775-1787 (2010).
538 40. C. Shen, Z. Shao, J. A. Powell-Coffman, The Caenorhabditis elegans rhy-1 gene
539 inhibits HIF-1 hypoxia-inducible factor activity in a negative feedback loop that does
540 not include vhl-1. *Genetics* **174**, 1205-1214 (2006).
541 41. D. K. Ma, R. Vozdek, N. Bhatla, H. R. Horvitz, CYSL-1 interacts with the O2-sensing
542 hydroxylase EGL-9 to promote H2S-modulated hypoxia-induced behavioral
543 plasticity in C. elegans. *Neuron* **73**, 925-940 (2012).
544 42. R. Kaletsky *et al.*, Transcriptome analysis of adult Caenorhabditis elegans cells
545 reveals tissue-specific gene and isoform expression. *PLoS Genet* **14**, e1007559
546 (2018).
547 43. H. Hutter, J. Suh, GExplore 1.4: An expanded web interface for queries on. *Worm* **5**,
548 e1234659 (2016).
549 44. J. S. Gilleard, J. D. McGhee, Activation of hypodermal differentiation in the
550 Caenorhabditis elegans embryo by GATA transcription factors ELT-1 and ELT-3. *Mol*
551 *Cell Biol* **21**, 2533-2544 (2001).
552 45. G. Broitman-Maduro, S. Sun, T. Kikuchi, M. F. Maduro, The GATA factor ELT-3
553 specifies endoderm in Caenorhabditis angaria in an ancestral gene network.
554 *Development* **149** (2022).
555 46. J. S. Gilleard, Y. Shafi, J. D. Barry, J. D. McGhee, ELT-3: A Caenorhabditis elegans
556 GATA factor expressed in the embryonic epidermis during morphogenesis. *Dev Biol*
557 **208**, 265-280 (1999).
558 47. J. H. Shinn-Thomas, J. J. del Campo, J. Wang, W. A. Mohler, The EFF-1A Cytoplasmic
559 Domain Influences Hypodermal Cell Fusions in C. elegans But Is Not Dependent on
560 14-3-3 Proteins. *PLoS One* **11**, e0146874 (2016).
561 48. K. S. Ghanta, T. Ishidate, C. C. Mello, Microinjection for precision genome editing in.
562 *STAR Protoc* **2**, 100748 (2021).
563 49. D. M. Parker, L. P. Winkenbach, A. Parker, S. Boyson, E. O. Nishimura, Improved
564 Methods for Single-Molecule Fluorescence In Situ Hybridization and
565 Immunofluorescence in Caenorhabditis elegans Embryos. *Curr Protoc* **1**, e299
566 (2021).
567 50. A. Dobin *et al.*, STAR: ultrafast universal RNA-seq aligner. *Bioinformatics* **29**, 15-21
568 (2013).
569 51. R. Patro, G. Duggal, M. I. Love, R. A. Irizarry, C. Kingsford, Salmon provides fast and
570 bias-aware quantification of transcript expression. *Nat Methods* **14**, 417-419 (2017).
571 52. S. Anders, P. T. Pyl, W. Huber, HTSeq--a Python framework to work with high-
572 throughput sequencing data. *Bioinformatics* **31**, 166-169 (2015).
573 53. N. Tsanov *et al.*, smiFISH and FISH-quant - a flexible single RNA detection approach
574 with super-resolution capability. *Nucleic Acids Res* **44**, e165 (2016).
575 54. M. Pujato, F. Kieken, A. A. Skiles, N. Tapinos, A. Fiser, Prediction of DNA binding
576 motifs from 3D models of transcription factors; identifying TLX3 regulated genes.
577 *Nucleic Acids Res* **42**, 13500-13512 (2014).
578 55. F. Ramírez *et al.*, deepTools2: a next generation web server for deep-sequencing
579 data analysis. *Nucleic Acids Res* **44**, W160-165 (2016).

580